Environmental Science and Pollution Research (2020) 27:43769–43785
https://doi.org/10.1007/s11356-020-10292-3

RESEARCH ARTICLE

Arsenite oxidation and arsenic adsorption on birnessite in the absence and the presence of citrate or EDTA

Mengyu Liang [1,2] · Huaming Guo [1,2] · Wei Xiu [3]

Received: 20 March 2020 / Accepted: 27 July 2020 / Published online: 1 August 2020

Abstract

Birnessite not only oxidizes arsenite into arsenate but also interacts with organic matter in various ways. However, effects of organic matter on interaction between As and birnessite remain unclear. This study investigated effects of citrate and EDTA (3.12 and 2.05 mM, respectively) on oxidation of As(III) (1.07 mM) and adsorption of As(V) (0.67 mM) on birnessite (5.19 mM as Mn) at near-neutral pH. We found that As(V) adsorption on birnessite was enhanced by citrate and EDTA, which resulted from the increase in active adsorption sites via dissolution of birnessite. In comparison with citrate batches, more As was adsorbed on birnessite in EDTA batches, where dissolved Mn was mainly presented as Mn(III)-EDTA complex. Citrate or EDTA-induced dissolution of birnessite did not decrease the As(III) oxidation rate in the initial stage where As(III) oxidation rate was rapid. Afterwards, As(III) oxidation was conspicuously suppressed in citrate-amended batches, which was mainly attributed to the decrease in adsorption sites by adsorption of citrate/Mn(II)-citrate complex. This suppression was enhanced by the increase in concentrations of dissolved Mn(II). Citrate inhibited As adsorption after As(III) oxidation due to the strong competitive adsorption of citrate/Mn(II)-citrate complex. However, the As(III) oxidation rate was increased in EDTA-amended batches in the late stage, which mainly derived from the increase in the active sites via birnessite dissolution. The strong complexation ability of EDTA led to formation of Mn(III)-EDTA complex. Arsenic adsorption was not affected due to the limited competitive adsorption of the complex on the solid. This work reveals the critical role of low molecular weight organic acids in geochemical behaviors of As and Mn in aqueous environment.

Keywords Adsorption · Arsenic · Birnessite · Citrate · EDTA · Oxidation · Reductive dissolution

Introduction

Manganese (Mn) oxides are widespread in terrestrial and aquatic environments as nodules and crusts (Zhang et al. 2008). They have several basic crystal structures (tunnel structures, layer structures, and spinel structures), usually with MnO_6 octahedron (Zhang et al. 2008; Si et al. 2015). Birnessite, as a layered Mn oxide, is one of the most common Mn oxide/hydroxide minerals in environment (Kwon et al. 2009), which has been extensively studied (Manceau et al. 2002; Zhu et al. 2010; Zhao et al. 2016; Li et al. 2019).

Birnessite is known to be a metal scavenger (Wang et al. 2012; Winkel et al. 2013; Li et al. 2019; Sun et al. 2019) due to its negative structural charges arising from vacancies and particle edges (including Zn(II), Ni(II), Pb(II)) (Wang et al. 2017). Since the point of zero charge pH (pH_{pzc}) of birnessite ranges from 1.4 to 4.5 (Stone and Ulrich 1989; Allard et al. 2017), it is normally negatively charged at the circumneutral pH and therefore is conducive to adsorb cations. In addition,

Responsible editor: Ioannis A. Katsoyiannis

Electronic supplementary material The online version of this article (https://doi.org/10.1007/s11356-020-10292-3) contains supplementary material, which is available to authorized users.

✉ Huaming Guo
hmguo@cugb.edu.cn

[1] State Key Laboratory of Biogeology and Environmental Geology, China University of Geosciences, Beijing 100083, People's Republic of China

[2] MOE Key Laboratory of Groundwater Circulation & Environment Evolution & School of Water Resources and Environment, China University of Geosciences (Beijing), Beijing 100083, People's Republic of China

[3] Institute of Geosciences, China University of Geosciences (Beijing), Beijing 100083, People's Republic of China

due to their low surface charge, high specific surface area, and polymorphic structures, Mn oxides have been employed to remove oxyanions from solutions (Gheju et al. 2016). Molecular-scale studies showed that the synthetic δ-MnO_2 usually in the form of birnessite adsorbs metals and metalloids (Lafferty et al. 2010a, 2010b) mainly by forming triple-corner-sharing (TCS) inner sphere complexes (Lafferty et al. 2010b; Parikh et al. 2010; Zhang and Sun 2013; Wang et al. 2018b).

Additionally, birnessite is a strong oxidant of chemical species such as As(III), Fe(II), and organic pollutants (Sun et al. 2019), due to the high oxidizing potential of tetravalent Mn (Mn(IV)) (Wang et al. 2018a, 2018b). Birnessite leads to the transformation of Fe(II) to Fe(III) oxides (Mock et al. 2019). Usually, As(III) is chemically oxidized to As(V) in minutes to hours with the reduction of birnessite to Mn(II) (Oscarson et al. 1983; Owings et al. 2019). Since arsenite (As(III)) is more toxic than arsenate (As(V)) (Petrick et al. 2000; Guo et al. 2014a), the oxidation of As(III) by birnessite helps detoxification of As in the environment (Chiu and Hering 2000; Tournassat et al. 2002). Two mechanisms have been proposed for the reactions between Mn oxides and As(III) under controlled laboratory conditions. The two-electron transfer step involves two electrons from one As(III) to one Mn(IV), forming Mn^{2+} and $H_2AsO_4^-$ (Eq. (1)) (Scott and Morgan 1995; Lafferty et al. 2010b), which dominates the rapid As(III) oxidation (Lafferty et al. 2010a, 2010b). However, the two one-electron transfer includes reduction of Mn(IV) to MnOOH (Eq. (2)), followed by As(III) oxidation by two MnOOH intermediate species (Eq. (3)) (Lafferty et al. 2010a, 2010b).

$$Mn^{IV}O_2 + H_3As^{III}O_3 + H^+ \rightarrow Mn^{II}(aq) + H_2As^{V}O_4^- + H_2O \quad (1)$$

$$2Mn^{IV}O_2 + H_3As^{III}O_3 + H_2O \rightarrow 2Mn^{III}OOH + H_2As^{V}O_4^- + H^+ \quad (2)$$

$$2Mn^{III}OOH + H_3As^{III}O_3 + 3H^+ \rightarrow 2Mn^{II}(aq) + H_2As^{V}O_4^- + 3H_2O \quad (3)$$

During the interaction between As and Mn oxides, ions and organic matter may block reaction sites of Mn oxides. Cation (such as Ca^{2+}) and oxyanion (i.e., $H_2PO_4^-$/HPO_4^{2-}) were reported to compete with As(V) for sorption sites on Mn(IV) oxides, and PO_4^{3-} is more competitive than Ca^{2+} (Jackson and Miller 2000; Lafferty and Loeppert 2005; Parikh et al. 2010). Although the extent of As(III) oxidation was decreased by low concentration of PO_4^{3-}, the initial oxidation rate was less affected (Parikh et al. 2010). High concentrations of antibiotic tetracycline hydrochloride (TC) competed with As(III) for oxidation by Mn(IV) oxides, and thus decreased its removal efficiency (Wang et al. 2015).

Low molecular weight organic acids (LMWOAs), being produced by plants, bacteria, and fungi, are ubiquitous in aquatic environment (Hongve et al. 2000; Strathmann 2011; Zheng et al. 2019). Among LMWOAs, citrate is a widespread carboxylic acid, which directly reduces Mn oxides in aqueous environment and forms complexes with Mn species (Wang and Stone 2006a, 2006b; Huangfu et al. 2015; Jefferson et al. 2015). The S-shaped curve of dissolved Mn concentration was observed during the reaction between citrate and Mn(IV) oxides, and intermediate products (including MnII/III-citrate complexes) promoted the reduction of Mn(IV) oxides (Wang and Stone 2006b). In addition, ethylenediaminetetraacetic acid (EDTA) is well known as a chelating agent, complexing with metal ions (Cheng et al. 2019) and extracting solid-bound metals (Kim et al. 2018). It also promotes the dissolution of Mn(IV) oxides by forming the surface complexes (Pankratova et al. 2001; Zhang et al. 2018a, 2018b). The high valence of Mn compounds can also be reduced by EDTA to the low valence of Mn (Zhang et al. 2018a, 2018b).

Although many studies focused on As(III) oxidation by Mn(IV) oxides (Li et al. 2010; Parikh et al. 2010; Wang et al. 2013; Fischel et al. 2015; Wang et al. 2017, 2018a, 2018b) and organic matter-induced dissolution of Mn(IV) oxides (Wang and Stone 2006a, 2006b; Huangfu et al. 2015; Zhang et al. 2018a, 2018b), no data are available for effects of LMWOAs on the interaction between As and Mn(IV) oxides. Understandings of the interaction among them are of great significance in revealing As transport and transformation in aqueous systems.

In this paper, effects of LMWOAs (i.e., citrate and EDTA) on As(III) oxidation and As(V) adsorption onto birnessite were investigated. We have found that reduction of birnessite by LMWOAs promotes adsorption of As(V), and EDTA further increases the oxidation kinetic rate of As(III) mainly through forming Mn(III)-EDTA complex. These results help to better understand As reactivity and mobility in the systems with Mn(IV) oxides and LMWOAs.

Materials and methods

Synthesis of birnessite

All chemicals were reagent grade, and all solutions were prepared with deionized (DI) water at room temperature (25 °C). Nanoflower-like birnessite was prepared by the facile hydrothermal reaction as described by Hou et al. (2014) with few modifications. The detailed procedure is shown as follows: 4.660 mL of $Mn(NO_3)_2$ (50 wt%) was diluted to 40 mL with DI water and transferred to a 100-mL Telfon bottle; 3.1608 g of $KMnO_4$ was added into $Mn(NO_3)_2$ aqueous solution. After sealed tightly, the bottle was kept in a water bath shaker at 160 rpm for 48 h at 50 °C. The black precipitate was obtained

as birnessite, which was washed with DI water and dried in a desiccator. The dried birnessite was crushed with an agate mortar and pestle for XRD, SEM, XPS, FTIR analysis, and batch experiments.

Reaction of As with birnessite

As(V) adsorption and As(III) oxidation/adsorption on birnessites were conducted at 25 °C. In order to reveal mechanisms of As reaction with birnessite, higher As concentrations were employed in relative to natural environments, but normally observed in thermal water. Solutions with 0.67 mM As(V) and 1.07 mM mg/L As(III) were prepared by diluting 5 g/L of As(V) stock solution and 8 g/L As(III) stock solution with acetate acid/sodium acetate buffer solution, respectively. Acetate acid/sodium acetate buffer solution (pH around 6.3), with the final concentration of acetate around 0.96 M, was prepared by dissolving 54.6 g sodium acetate and 20 mL 1 mM acetate acid in 500 mL DI water (Hou et al. 2016, 2017). Acetate was chosen since it has a weak tendency to form surface complexes with Mn(IV) oxides and is unable to be oxidized by Mn(IV) oxides (Chiu and Hering 2000).

Batch experiments were performed by suspending 0.03 g birnessite (0.6 g/L, equivalent to 5.19 mM Mn) in 50 mL As solution for 1440 min. For reactions with LMWOAs, 0.03-g citric acid or EDTA was added in the mixture (corresponding to 3.12 and 2.05 mM, respectively). Aliquots of about 2 mL suspension were taken and immediately filtered through a 0.22-μm membrane at predetermined time intervals (30, 60, 180, 360, 540, 720, 1080, 1440 min) to investigate the kinetics of As adsorption and As(III) oxidation. The filtered solutions were stored at 4 °C for analysis of total dissolved As, As speciation, dissolved Mn, and Mn speciation. Mn speciation was determined immediately after filtration in order to avoid change of Mn species (Oldham et al. 2017a, 2017b; Johnson et al. 2018). After reaction for 1440 min, suspensions were taken and centrifuged at 4000 rpm to separate solid particles from solutions. Solid samples were washed with DI water and freeze-dried for XRD, SEM, XPS, and FTIR analysis. LMWOA-free batches (Controls) were also carried out without addition of LMWOAs. Solution pH was well-buffered at 6.3 ± 0.1 during the experiments. Duplicate experiments were conducted for all treatments.

Water analysis

Total dissolved As and Mn concentrations were measured with and inductively coupled plasma-atomic emission spectrometer (ICP- AES, iCAP6300, Thermo) with the detection limits of 10 μg/L. Dissolved As speciation was analyzed with a high-performance liquid chromatography-hydride generation-atomic fluorescence spectrophotometer (HPLC-HG-AFS, Jitian Corp., Beijing), and the detection limit for As(III) and As(V) was 2 μg/L (Guo et al. 2014b).

Dissolved Mn speciation was analyzed according to the method developed by Madison et al. (2011), with the detection limit around 50 nM. A 0.2 mM α, β, γ, and δ-tetrakis (4-carboxyphenyl)porphine [T-(4-CP)P] solution was prepared by dissolving 79.1 mg T-(4-CP)P in 5 mL 0.1 M NaOH and diluting to 500 mL with DI water. Cadmium chloride ($CdCl_2$) stock solution (0.12 mM) was prepared by dissolving 0.022 g of $CdCl_2$ in 100 mL DI water. A buffer solution was prepared by mixing 50 mL of 0.025 M sodium tetraborate decahydrate, 20 mL of 0.1 M hydrochloric acid (HCl), and 25 mL of 0.6 M imidazole. Mn(II) standard solutions were prepared from Mn(II) chloride ($MnCl_2$) salt (analytical reagent). A UV-visible absorbance spectroscopy (UV-vis) (UV1800, LabTech Ltd.) was used to analyze Mn speciation. We added 120-μL buffer solution, 60-μL $CdCl_2$, 360-μL T-(4-CP)P solution, 100-μL sample, and 2360-μL DI water sequentially in a 1-cm path length quartz cuvette. Both Mn(II) and Mn(III) react with T(4-CP)P to form Mn(III)-T(4-CP)P with the peak absorbance wavelength of 468 nm by ligand exchange, but the formation rate of Mn(III)-T(4-CP)P from Mn(III) species is slower than from Mn(II) species (Luther et al. 2015). Therefore, total dissolved Mn concentration can be expressed as Eq. (4).

$$\begin{aligned}[\mathrm{Mn}]\mathrm{Total} &= [\mathrm{Mn(III)}{-}\mathrm{T(4{-}CP)P}]\mathrm{Total} \\ &= \mathrm{Mn(II)}_0\left(1{-}e^{-k_1 t}\right) + \mathrm{Mn(III)}_0\left(1{-}e^{-k_2 t}\right) \qquad (4)\end{aligned}$$

where $Mn(II)_0$, $Mn(III)_0$, k_1, and k_2 represent initial Mn(II) and Mn(III) concentrations and the rate constants of the Mn(II) and Mn(III) complex formations, respectively. A program using a nonlinear least square minimization approach written in the MATLAB was used to determine initial concentrations of Mn(II) and Mn(III) by optimizing the original absorbance-time kinetic scan data obtained from a spectrophotometer (Fig. S1). The sums of dissolved Mn(II) and Mn(III) concentrations are well in line with total dissolved Mn concentrations measured by ICP-AES (Fig. S2).

Solid analysis

The crystallinity of synthetic birnessite was characterized by synchrotron X-ray diffraction (μ-XRD). μ-XRD was performed at 10 keV ($k = 0.6199$ Å) at the beamline BL15U at SSRF and equipped with a Si(111) monochromator. μ-XRD data were analyzed using MDI Jade (Version 6).

The freeze-dried samples were first placed in Quorum SC7620 Sputter Coater for platinum treatment, and then analyzed by scanning electronic microscopy (SEM) (Zeiss Supra 55 SAPPHIRE). The surface elemental compositions and O and Mn species of pristine and used birnessite were

determined with scanning imaging X-ray photoelectron spectrometer (XPS) (PHI Quantera SXM, Japan ULVAC-PHI), with a monochromatized AlKα X-ray source and base pressure less than 1×10^{-7} Torr in the analytical chamber. The spot size was 200 μm and the electron beam incident angle was fixed at 45°. Survey scans were recorded from 0 to 1200 eV using a fixed pass energy of 280 eV with a step size of 1.0 eV, whereas narrow scans were collected using a fixed pass energy of 55 eV with a step size of 0.1 eV. The accuracy is ± 0.01 eV. Fourier transform infrared spectra (FTIR) for birnessite were collected on an American PerkinElmer spectrum using compressed KBr disc technique in the range of 400–4000 cm^{-1} with a resolution of 1 cm^{-1}. Solid samples were digested by dissolving 0.1-g sample in 0.25-M hydroxylamine hydrochloride, and then analyzed for Mn contents by ICP-AES.

Results

Characterization of synthetic birnessite

The XRD spectra show five diffraction peaks at 1.22, 1.41, 2.43, 3.64, and 7.33 Å (Fig. S3), which are similar to birnessite reported by Gao et al. (2015). The five peaks are in good agreement with the standard data of synthetic birnessite from JCPDS card no. 86-0666 (Gao et al. 2015). The data reveal that the synthesized sample was in the form of birnessite.

The SEM images show the nanoflower-like birnessite with an average size of 0.5 nm and porous surface (Fig. 1). Similar morphology was obtained by Hou et al. (2017) and Swetha et al. (2018). It was reported that nanoflowers were built from dozens of nanoleaves (Ahmed and Huang 2014).

Results of XPS broad scans are shown in Fig. 2. It illustrates that Mn, O, and K existed in the birnessite structure.

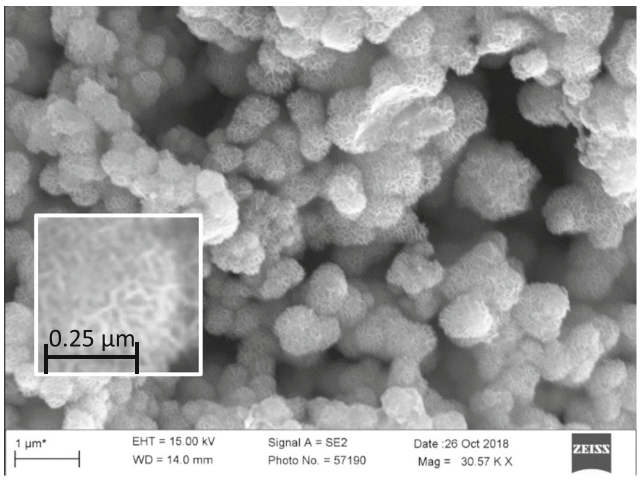

Fig. 1 SEM images of the pristine birnessite

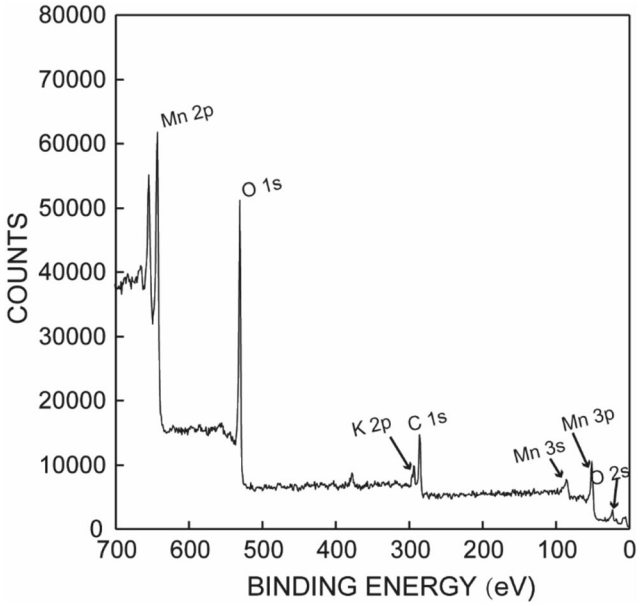

Fig. 2 XPS broad scans of the pristine birnessite

Content of Mn in birnessite was 57%, being higher than bulk content of 47.5% determined by the hydroxylamine hydrochloride method. The possible reason was that XPS spectra reflect Mn content of the mineral surface, instead of bulk content.

The interpretation of Mn(2p) spectra is complicated by multiplet peaks, showing that the unusual broadening was the result of high spin states of Mn(II), Mn(III), and Mn(IV) (Nesbitt et al. 1998). The Mn($2p_{3/2}$) spectra had a broad shoulder at high binding energy with the maximum near 642.8 eV, and a trailing in the range of 644 to 647 eV (Fig. 3a). Using the multiplet fitting of the Mn($2p_{3/2}$) peaks, the relative contents of Mn(II), Mn(III), and Mn(IV) in birnessite were determined to be 3.24%, 40.5%, and 56.3%, respectively (Table 1), with the average oxidation state (AOS) of 3.53, which correspond with the previous work (Boumaiza et al. 2019). The O(1s) spectra of the birnessite had a maximum near 529.8 eV (Fig. 3b). Three species of oxygen (including lattice oxygen O^{2-}, hydroxide oxygen OH^-, and oxygen in molecular water) were recognized from the broad shoulder and the pronounced tail at high binding energy (Wang et al. 2012; Jefferson et al. 2015). Lattice oxygen was the main oxygen species with content of 78.1% (Table S1), being consistent with the previous study (Banerjee and Nesbitt 2001), while OH^- and oxygen in molecular water accounted for 11.3% and 10.7%, respectively (Table S1, S2). All spectra were well-fitted using a 70:30 Gaussian: Lorentzian peak shape.

The FTIR spectra show that the stretching vibration of free hydroxyl groups on the mineral surface resulted in a band center at 3402 cm^{-1}; the bending vibrations of H-O-H of adsorbed H_2O had a peak at 1629 cm^{-1}; and the vibration of surface hydroxyl group (Mn-OH) within the mineral was peaked at 1038 cm^{-1} (Fig. 4) (Liu et al. 2009; Guan et al.

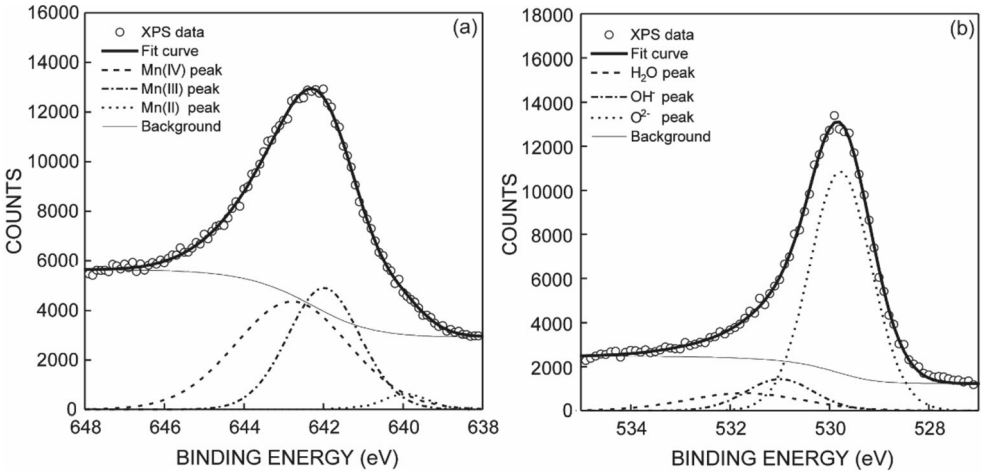

Fig. 3 Mn($2p_{3/2}$) spectra (**a**) and O(1s) spectra (**b**) of the pristine birnessite

2017; Zhang et al. 2018a, 2018b). The absorbing peaks at 720, 582, 521, and 477 cm^{-1} may correspond to the stretching vibration of Mn-O-Mn in the birnessite (Guan et al. 2017; Ling et al. 2017; Zhang et al. 2018a, 2018b).

As(V) adsorption in the absence and the presence of LMWOAs

Changes in concentrations of As(V) and total dissolved Mn over time during the experiments are shown in Fig. 5. Two stages (quick As adsorption/birnessite dissolution and adsorption/birnessite dissolution equilibrium) were obtained in controls (LMWOA-free batches) and EDTA-amended batches, while three stages were observed in citrate-amended batches, including quick As(V) adsorption/birnessite dissolution, As(V) adsorption equilibrium and continuous dissolution of birnessite, and equilibrium of birnessite dissolution.

As(V) adsorption in the control batches reached equilibrium in 30 min with the low adsorption of 34.0 μmol/g and adsorption efficiency of only 2.95%. In EDTA-amended batches, adsorption of As(V) reached equilibrium at 360 min with the highest adsorption efficiency around 11.83%. At the second stage, As(V) adsorption reached equilibrium (Fig. 5a); total dissolved Mn reached a maximum of 1730 μM. Dissolved Mn was mostly in the species of Mn(III) in EDTA batches (Fig. 5b), which was generally presumed as Mn(III)-complexes.

For citrate-amended batches, As concentrations generally remained constant after the first stage at around 180 min, and the adsorption efficiency was lower than that in EDTA-amended batches and higher than that in controls. During the second stage, birnessite was dissolved continuously. Concentration of total dissolved Mn was extremely high, reaching 2840 μM at the third stage after As(V) adsorption equilibrium. Around two-thirds of dissolved Mn were in the species of Mn(III), being considered as Mn(III)-citrate complex.

Table 1 Results of XPS Mn($2p_{3/2}$) and O(1s) multi-peak fitting of the pristine birnessite

Peak	B.E(eV)	FWHM(eV)	Percent [(a)](%)
Mn($2p_{3/2}$) parameters			
Mn(II)	639.93	1.35	3.24
Mn(III)	641.99	2.15	40.49
Mn(IV)	642.79	3.35	56.27
O(1 s) parameters			
O^{2-}	529.76	1.46	78.05
OH^-	530.80	1.59	11.25
H_2O	531.70	2.75	10.70

[(a)] The percent represents the contribution of each peak to the total number of counts under Mn ($2p_{3/2}$) and O(1s) peaks

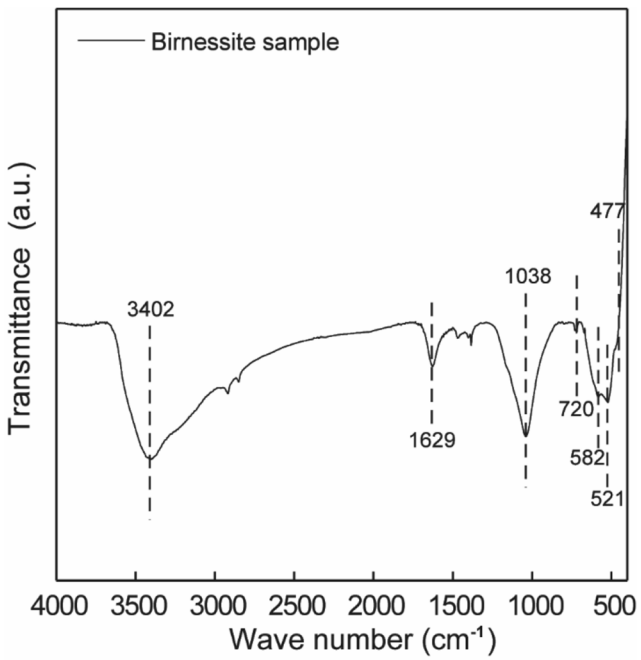

Fig. 4 FTIR spectra of the pristine birnessite

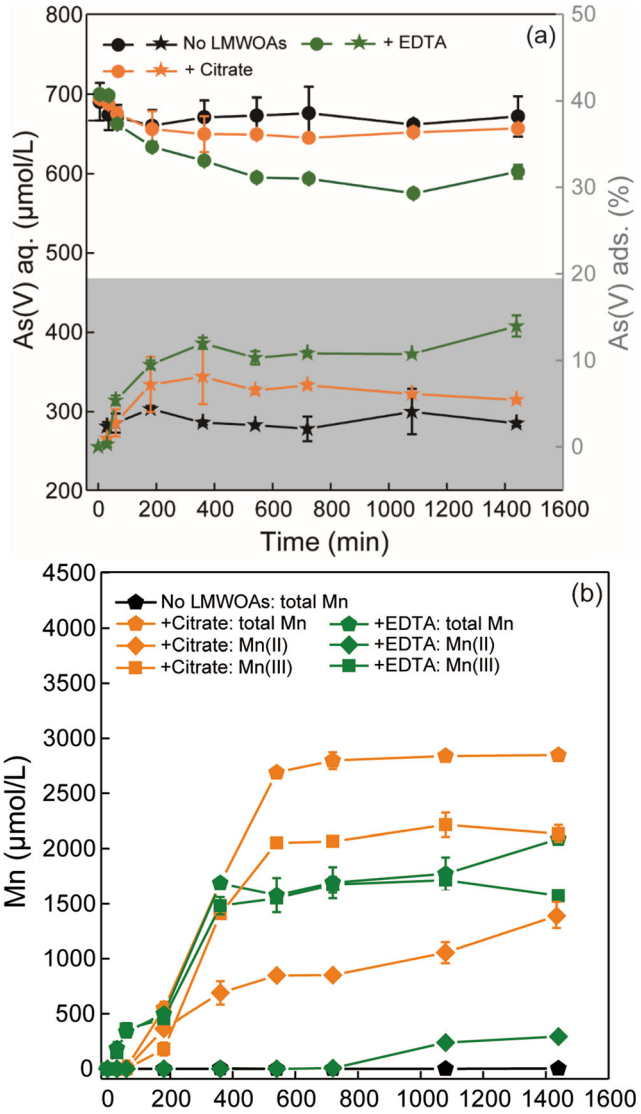

Fig. 5 Variations in As(V) concentrations and adsorption (**a**) and dissolved Mn, Mn(II), and Mn(III) concentrations (**b**) during experiments with 50 mg/L As(V) and 0.6 g/L birnessite for 24 h at pH 6.3 (data are partially quoted from Liang et al. 2019)

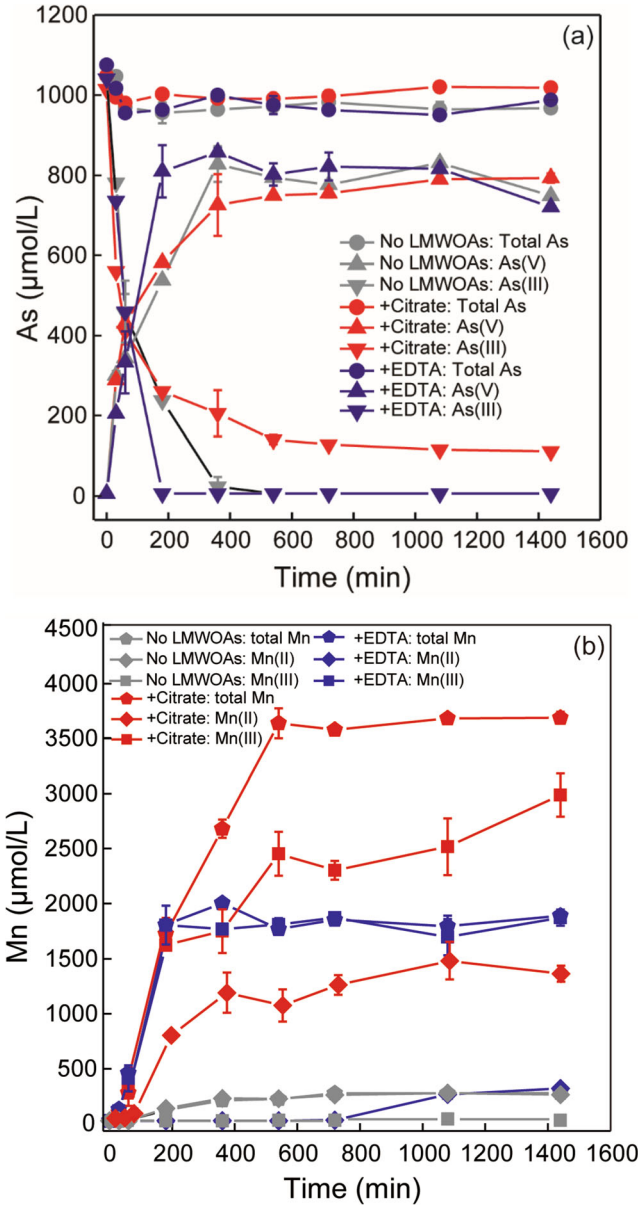

Fig. 6 Variations in dissolved As(III), As(V), and total dissolved As concentrations (**a**) and dissolved Mn, Mn(II), and Mn(III) (**b**) in batch experiments with 80 mg/L As(III) and 0.6 g/L birnessite for 24 h at pH 6.3 (data are partially quoted from Liang et al. 2019)

As(III) oxidation and adsorption in the absence and the presence of LMWOAs

LMWOAs not only affected As adsorption but also controlled As(III) oxidation. There were three clear As(III) oxidation stages in the experiments (Fig. 6a). In the first stage (before 60 min), the oxidation was rapid. Then, the second stage was characterized by the decrease in the oxidation rate. In the third stage, As(III) oxidation was in equilibrium. Generally, As(III) decreased according to an exponential decay in all experiments (Fig. 6a). Since As(III) was rapidly oxidized into As(V) by birnessite and the adsorbed As fraction only consisted of As(V) (Owings et al. 2019), the decrease in dissolved As(III) reflects the oxidation rate of As(III) in the systems.

In the first stage, the oxidation of As(III) showed no difference among three batches (Fig. 6a; Table 2). As(III) concentrations decreased to 588 μM, 605 μM, and 584 μM in

Table 2 Changes in concentrations of dissolved As(III) and As(V) during the first stage of the reaction between As(III) and birnessite

	The decrease in As(III)	The increase in As(V)
Birnessite +As(III)	588 μM	340 μM
Birnessite +As(III)+citrate	605 μM	427 μM
Birnessite +As(III)+EDTA	584 μM	328 μM

control, citrate-amended, and EDTA-amended batches, respectively. Dissolved As(V) concentrations increased in all batches, and slightly higher concentrations of As(V) and total As were found in citrate-amended batches (Fig. 6a; Table 2). Figure 6b reveals that there was less dissolved Mn compared with the amount of dissolved As(V).

In the second stage, the rate of As(III) oxidation decreased and high concentrations of dissolved Mn were detected (Fig. 6). No evident changes in total As concentration were observed, and As adsorption reached equilibrium in all batches, showing no significant differences between the different batches. However, variation trends in As(III) and As(V) concentrations were obviously different among those three batches (Fig. 6a). It is clear that the EDTA-amended batches had the fastest As(III) oxidation rate, followed by the control batches and the citrate-amended batches. It indicates that citrate inhibited As(III) oxidation, while EDTA promoted the oxidation in relative to control experiments. During this stage, total dissolved Mn concentrations in citrate-amended batches were significantly higher than those of controls and EDTA-amended batches. Around two-thirds of dissolved Mn were in the species of Mn(III) in citrate-amended batches, while dissolved Mn mostly (> 80%) existed as Mn(III) species in EDTA-amended batches (Fig. 6b). Dissolved Mn in controls was mostly in the species of Mn(II), as reported previously (Scott and Morgan 1995; Owings et al. 2019).

In the third stage, both dissolved As and Mn concentrations kept stable (Fig. 6). Total dissolved Mn reached maximum concentrations of 253, 3660, and 1840 μM in control, citrate-amended, and EDTA-amended batches, respectively. The molar ratio of removed As to dissolved Mn (Asrem/Mnprod = 1.04/0.25) in control was > 1, which suggests that Eqs. (2) and (3) should be taken into account, in addition to Eq. (1). It means that birnessite was probably partially reduced to Mn(III). Moreover, a fraction of Mn(II) was adsorbed or incorporated onto/in the crystal lattice (Fischel et al. 2015), which could be another cause for the high molar ratio. However, higher concentrations of total dissolved Mn were observed in LMWOA-amended batches with lower Asrem/Mnprod (0.25 and 0.57 in citrate-amended batches and EDTA-amended batches, respectively). It indicates that, in addition to dissolved Mn produced by redox reaction between As(III) and MnO_2, there was an extra source of dissolved Mn in LMWOA-amended batches. Moreover, a slight increase in total dissolved As concentration in the citrate-amended batch was observed during this stage (Fig. 6a).

Birnessite characterization after reactions

A great change in the surface morphology was found in citrate-amended As(V)/As(III) experiments, showing that the structural integrity decreased with holes on the spherical particles (Fig. 7c, d). For control and EDTA-amended batches, the morphology was not significantly altered (Fig. 7a–f). The monotonous morphology of the minerals indicates that no phase transformations occurred during experiments.

Mn($2p_{3/2}$) narrow scans of used birnessite are shown in Fig. 8. The fitting results reveal that the proportions of Mn species near the surface had no detectable changes. The relative proportions of Mn(II), Mn(III), and Mn(IV) are listed in Table 3 for pristine and used birnessite. It shows that variations in the percentages of Mn(IV), Mn(III), and Mn(II) in the used samples were less than 5% in comparison with the original birnessite (Table 3), although some Mn was transferred from solid to solution. The Mn($2p_{3/2}$) spectra of birnessite in As(III) experiments demonstrate that Mn(III) content increased from 40 to 45% in citrate-amended batches.

The O(1s) spectra of the used birnessite are illustrated in Fig. 9. Decreasing trends in contents of lattice oxygen and increasing trends in oxygen contents in molecular water were observed in all batches compared with the original birnessite (Table S1), which are in line with previous data (Cheng et al. 2019; Liu et al. 2019). Those trends were the most evident in the citrate-amended experiments, where the lattice oxygen decreased by 27.42% in As(V) batches and 22.21% in As(III) batches, and the proportion of oxygen in molecular water increased by 31.4% and 22.21%, respectively (Table S1).

Discussion

Effects of LMWOAs on As(V) adsorption on birnessite

Roles of LMWOAs on As(V) adsorption in As(V) batches

Experimental data show that As(V) adsorption on birnessite quickly reached equilibrium with low adsorption capacity in all-studied systems (Fig. 5a). As(V) adsorption on the active sites of birnessite was limited due to its negatively charged form ($H_2AsO_4^-$) and the overall negative surface of Mn oxides at neutral pH (Lafferty et al. 2010a, 2010b; Villalobos et al. 2014). LMWOAs played an important role in controlling As adsorption on binessite. The relatively higher adsorption was obtained in the LMWOA-amended experiments (Fig. 5a), where higher total dissolved Mn was detected. It indicates that the dissolution of birnessite was conducive to As(V) adsorption. Previous studies have shown that redox reaction induces surface alteration and creates fresh reaction sites for As(V) adsorption on Mn(IV) oxide surfaces (Parikh et al. 2008; Lafferty et al. 2010a, 2010b). The highest concentrations of total dissolved Mn (2840 μM) were observed in citrate-amended experiments. S-shaped curve of dissolved Mn concentrations with the initial slow increase followed by a sharp increase is in accordance with the previous study (Wang and Stone 2006b), which would be attributed to the autocatalysis.

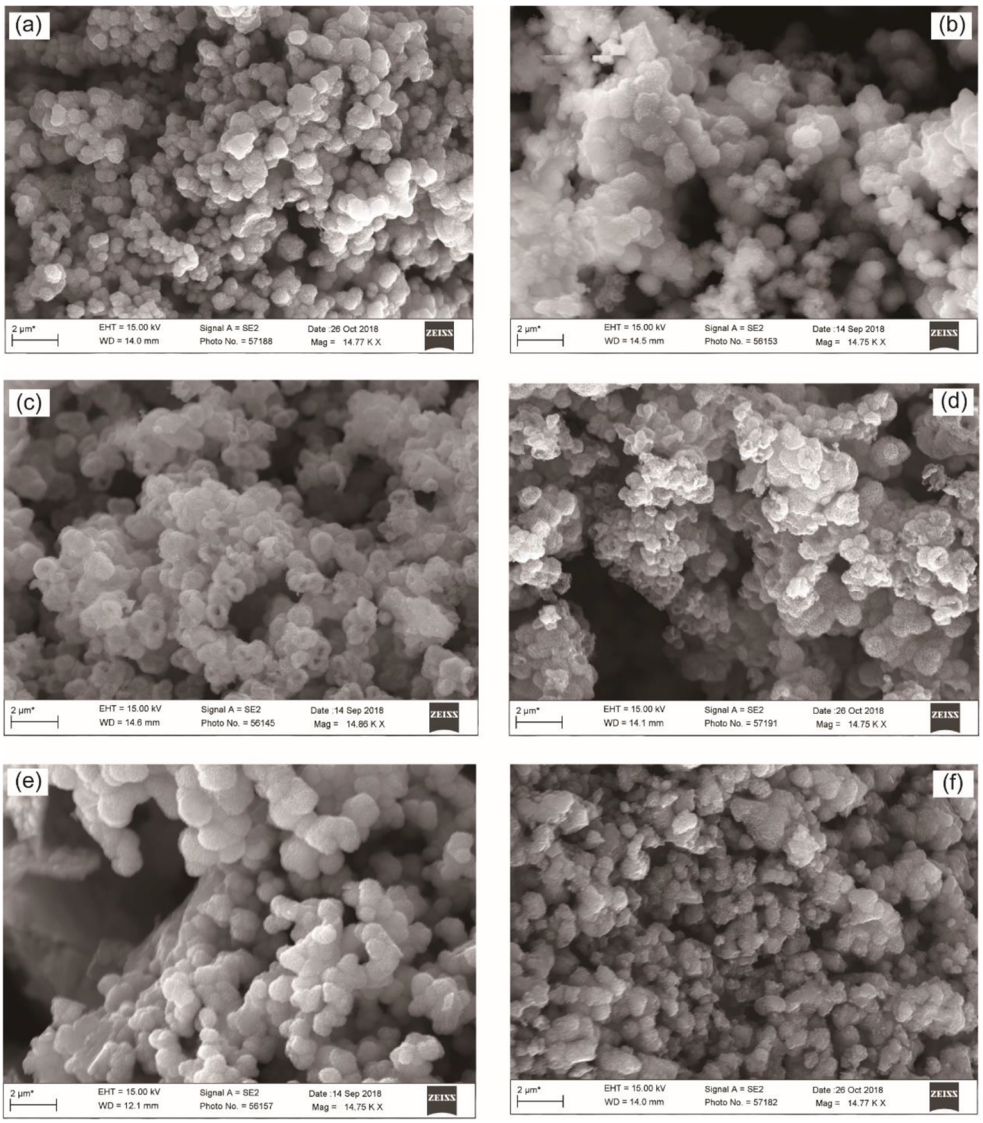

Fig. 7 SEM images of used birnessite after As(V) adsorption ((**a**) MnO_2+As(V); (**c**) MnO_2+As(V)+citrate; (**e**) MnO_2+As(V)+EDTA) and As(III) oxidation ((**b**) MnO_2+As(III); (**d**) MnO_2+As(III)+citrate; (**f**) MnO_2+As(III)+EDTA)

To be more specific, the initial slow increase was related to citrate as the only reductant during the redox reaction with birnessite; and the sharp increase resulted from a strong positive feedback generating a large amount of dissolved Mn. The positive feedback involves the process that electrons are transferred from Mn(II)-citrate complex to surface-bound Mn(III/IV) (Wang and Stone 2006b; Jefferson et al. 2015; Allard et al. 2017). To further describe the reaction, Mn(IV) reduction and electron transfer were calculated according to Wang et al. (2018a, 2018b), showing that approximately 2-mol electrons were transferred from per mole of citrate to birnessite, which is consistent with the previous studies (Wang and Stone 2006a, 2006b). It also indirectly proves that citrate experienced the incomplete mineralization since the theoretical maximum electron transfer per mole of citrate is 18 mol (Flynn and Catalano 2019). In comparison with citrate-birnessite batches, lower concentrations of total dissolved Mn were observed in citrate-birnessite-As(V) batches (Fig. 10a), which indicates that the reaction between citrate and birnessite was affected by As(V). Since the active sites were required for both citrate/Mn(II)-citrate complex and As(V) on birnessite, there was a competitive adsorption between As(V) and citrate/Mn(II)-citrate complex (Wang et al. 2016). In other words, the citrate-induced dissolution was suppressed in the presence of As(V). Since citrate has two or three negative charges at pH 6.3 (Madurga et al. 2017), Mn(II)-citrate complex, having a ratio of citrate to metal ion of 1:1 (Kachhawaha and Bhattacharya 1962), is supposed to be electrically neutral or negative. Therefore, adsorption of this complex could affect As(V) adsorption. Although citrate/Mn(II)-citrate complex competed the surface sites with As(V), higher adsorption of As(V) (about 6.2%) was observed, which likely resulted from the new surface sites created by citrate-induced reductive dissolution in citrate-amended batches. Continuous dissolution of birnessite after As(V) adsorption equilibrium resulted in slight desorption of As, which was supported by the detectable

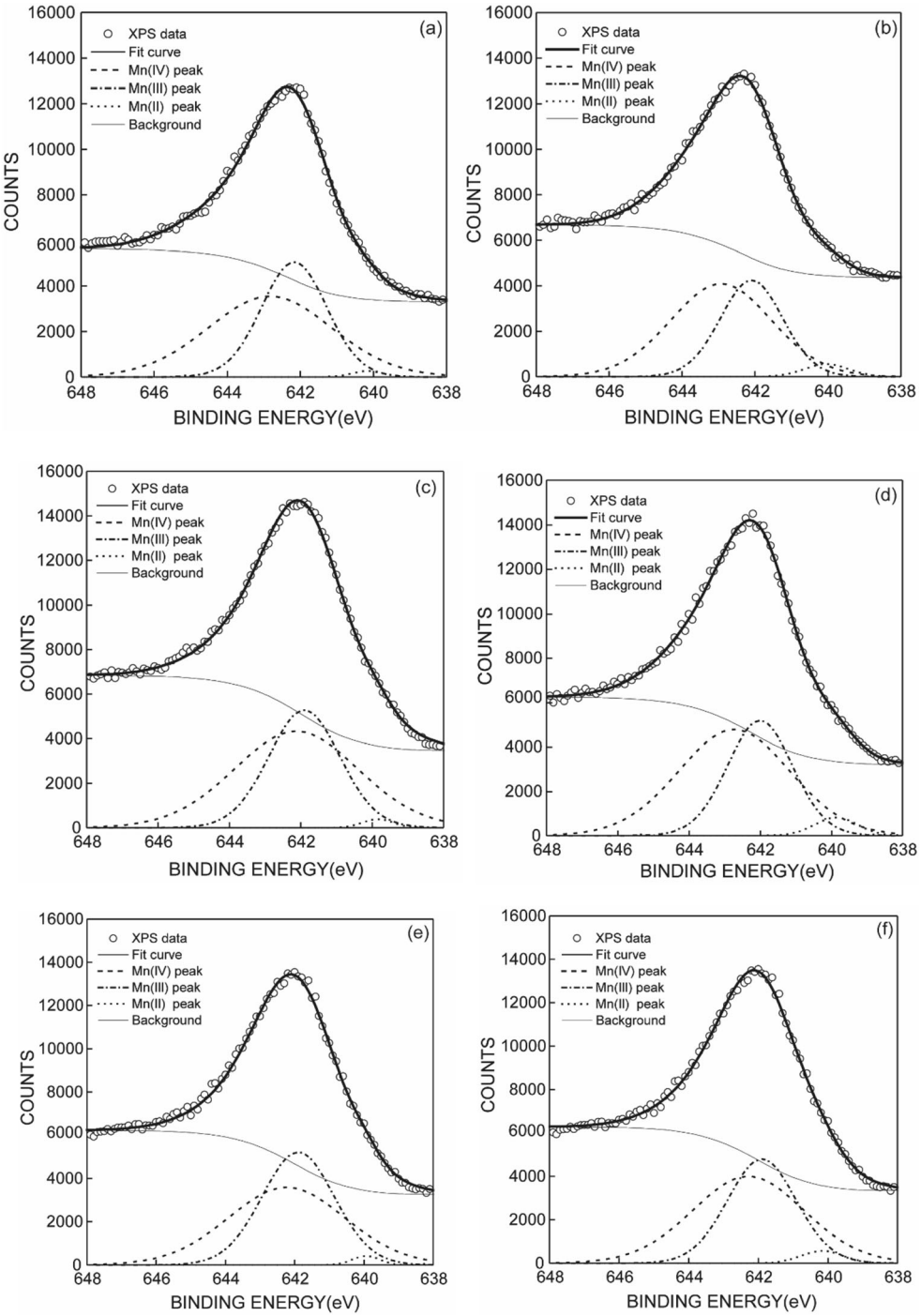

Fig. 8 Mn ($2p_{3/2}$) spectra of used birnessite and deconvolution peaks. **a**–**c** Mn ($2p_{3/2}$) spectra of the birnessite after As(V) adsorption in control, citrate-amended, and EDTA-amended batches, respectively. **d**–**f** Mn ($2p_{3/2}$) spectra of the birnessite after As (III) oxidation in control, citrate-amended, and EDTA-amended batches, respectively. Circles represent XPS data, and the thick solid curves represent the best fit to the XPS data. The dash lines represent Mn (IV) multiplet peaks, the dash-dot curves Mn (III) multiplet peaks, and the dotted curves Mn (II) multiplet peaks

change of mineral surface characteristics after 1440-min reaction (Fig. 7c).

Concerning EDTA-amended batches, total dissolved Mn was initially rapidly increased (Fig. 5b), which may be related to the fact that EDTA has a stronger complexing ability to promote dissolution of minerals due to its more carboxyl groups than citrate (Huangfu et al. 2015). Dissolution-induced active sites for As(V) adsorption were produced more efficiently at the beginning of the reaction, which resulted in higher As(V) adsorption in EDTA-amended batches. During the whole process, the mineral dissolution in EDTA-amended batches with 1730 μM mg/L dissolved Mn and around 1.8-mol electrons per mole of EDTA transferred to birnessite was not as high as those in citrate-amended batches. However, the ETDA-amended batches had the highest As adsorption capacity among all batches, where only Mn(III) was detected for most of time (Fig. 5b). In contrast to the competitive adsorption of Mn(II)-citrate complex on the surface of birnessite,

Table 3 Mn ($2p_{3/2}$) peak parameters for pristine and used birnessite

	Peak Mn(II) ($2p_{3/2}$) parameters	B.E(eV)	FWHM(eV)	Percent (%)
MnO_2	Mn(II)	639.93	1.35	3.24
MnO_2+As(V)	Mn(II)	640.10	1.03	1.15
MnO_2+As(V)+citrate	Mn(II)	640.04	1.43	3.51
MnO_2+As(V)+EDTA	Mn(II)	639.84	1.01	1.26
MnO_2+As(III)	Mn(II)	639.87	1.41	3.84
MnO_2+As(III)+citrate	Mn(II)	640.05	1.33	4.51
MnO_2+As(III)+EDTA	Mn(II)	640.17	1.42	2.99
	Mn(III)($2p_{3/2}$) parameters			
MnO_2	Mn(III)	641.99	2.15	40.49
MnO_2+As(V)	Mn(III)	642.17	2.11	42.30
MnO_2+As(V)+citrate	Mn(III)	642.10	2.02	37.69
MnO_2+As(V)+EDTA	Mn(III)	641.90	2.36	40.61
MnO_2+As(III)	Mn(III)	642.00	2.16	37.28
MnO_2+As(III)+citrate	Mn(III)	642.02	2.3	45.23
MnO_2+As(III)+EDTA	Mn(III)	641.9	2.32	41.16
	Mn(IV) ($2p_{3/2}$) parameters			
MnO_2	Mn(IV)	642.79	3.35	56.27
MnO_2+As(V)	Mn(IV)	642.83	4.00	56.55
MnO_2+As(V)+citrate	Mn(IV)	642.93	3.27	58.80
MnO_2+As(V)+EDTA	Mn(IV)	642.13	4.11	58.13
MnO_2+As(III)	Mn(IV)	642.72	3.7	58.88
MnO_2+As(III)+citrate	Mn(IV)	642.84	3.77	50.26
MnO_2+As(III)+EDTA	Mn(IV)	642.29	3.78	55.85

EDTA is presumed to limit the competition through stabilizing dissolved Mn as Mn(III)-EDTA complex (Table 3) (Prieto et al. 2013). Mn(II) (%) and Mn(III) (%) on used birnessite in EDTA batches were similar to those of the control batches (Table 3). Overall, the highest adsorption in EDTA-amended batches was related to the creation of adsorption sites via complexing dissolution and the limited competitive adsorption between As and Mn(III) complexes. The Mn(III) in solutions is assumed to be Mn(III)-LMWOA complex since the dissolved Mn(III) only stably exists as complex with ligands in aqueous environment (Duckworth and Sposito 2005, 2007; Oldham et al. 2015, 2017a, 2017b).

Roles of LMWOAs on As(V) adsorption in As(III) oxidation experiments

In As(III) batches, concentration of dissolved As(V) increased proportionally to the decrease in As(III), and total As decreased rapidly when the oxidation of As(III) by birnessite was rapid (Fig. 6a, Table 2). According to the previous studies, As(V) as the product of As(III) oxidation was first detached from the surface of the mineral and then partly readsorbed (Amirbahman et al. 2006). The decrease in total dissolved As was caused by As(V) adsorption (Lafferty et al. 2010a; Owings et al. 2019). Though the amount of oxidized As(III) was similar under all batches during this stage (Table 2), higher concentrations of dissolved As(V) were observed in citrate-amended batches than in other batches (Fig. 6a, Table 2), which indicates that Mn(II)-citrate complex inhibited As(V) adsorption through competing the adsorption sites with As(V). The inhibition of As(V) adsorption appeared earlier than the period when the As(III) oxidation rate was significantly reduced.

After the equilibrium of As(III) oxidation, increases in total dissolved As and As(V) were observed in citrate-amended batches (Fig. 6a), indicating that As(V) was partly desorbed into solution in the presence of citrate.

Roles of LMWOAs on As(III) oxidation

Birnessite showed a strong capacity for As(III) oxidation in all experiments (Fig. 6a). The data show that the As(III) oxidation initially proceeded rapidly, and then slowed down (Fig. 6a), which is in agreement with previous results (Tani et al.

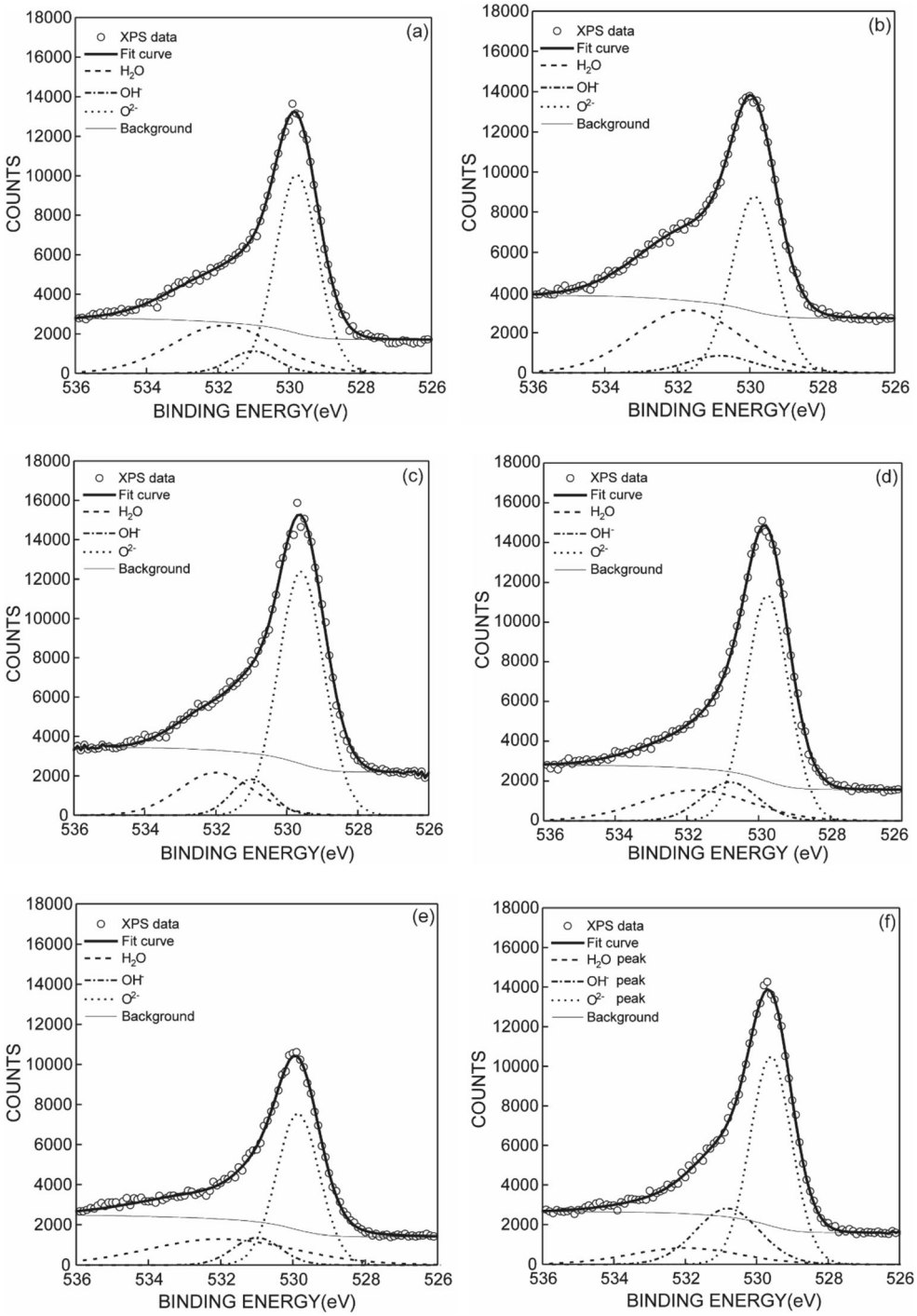

Fig. 9 O(1s) spectra of used birnessite and deconvolution peaks. **a**–**c** O(1s) spectra of the birnessite after As(V) adsorption in control, citrate-amended, and EDTA-amended batches, respectively. **d**–**f** O (1s) spectra of the birnessite after As (III) oxidation in control, citrate-amended, and EDTA-amended batches, respectively. Circles represent XPS data and the thick solid curve represents the best fit to the XPS data. The dash lines represent O^{2-} multiplet peaks, the dash-dot curves OH^- multiplet peaks, and the dotted curves H_2O multiplet peaks

2004; Parikh et al. 2008; Ginder-Vogel et al. 2009; Lafferty et al. 2010a, 2010b; Wang et al. 2017). The oxidation rate decreased since Mn(II), the product of Mn(IV) oxide reduction, was adsorbed on both edge and vacancy sites of the oxides and passivated Mn oxides (Villalobos et al. 2014; Fischel et al. 2015).

During the rapid oxidation stage, relatively low concentrations of total dissolved Mn in LMWOA-amended batches (Fig. 6b) were due to slow LMWOA-induced dissolution. Moreover, dissolved Mn was mostly in the species of Mn(III) complexes in LMWOA-amended batches (Fig. 6b), which would not be adsorbed on the surface as strongly as Mn(II). This stage was considered to be dominated by two-electron transfer step (Eq. (1)) (Lafferty et al. 2010b) and Mn(II) as the reduction products was adsorbed fully on the vacancy sites (Lafferty et al. 2010a, 2010b and 2011; Fischel et al. 2015). There was less dissolved Mn compared with the amount of dissolved As(V). The limited adsorption of As(V)

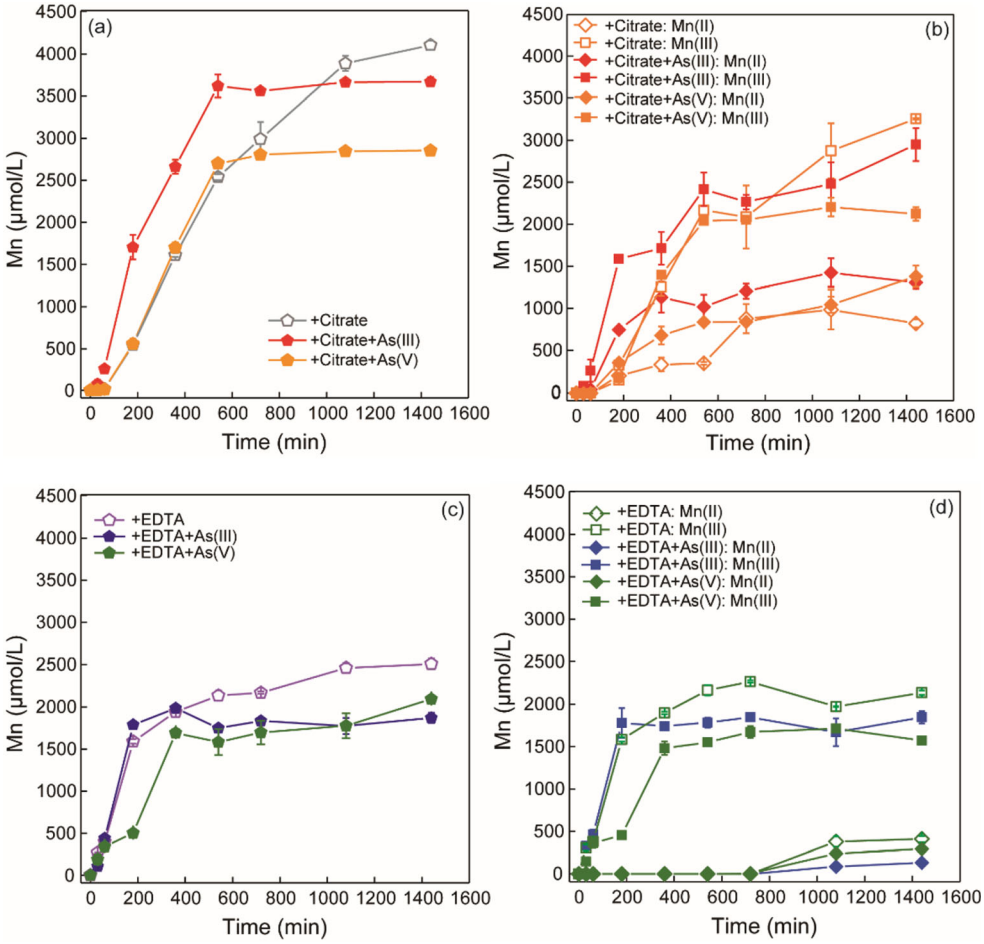

Fig. 10 Total dissolved Mn, dissolved Mn(II), and dissolved Mn(III) concentrations in solutions of citrate-amended batches (citrate-birnessite batches, citrate-birnessite-As(V) batches, citrate-birnessite-As(III) batches) and EDTA-amended batches (citrate-birnessite batches, citrate-birnessite-As(V) batches, citrate-birnessite-As(III) batches) for 24 h at pH 6.3

suggests that the majority of reduced Mn(II) was steadily readsorbed on the surface of birnessite (Owings et al. 2019). In addition, relative contents of Mn(III) had limited changes after reaction (< 5%) (Table 4). Therefore, we believe that the redox reaction between Mn(II) and birnessite was limited.

In the second stage, EDTA promoted As(III) oxidation, while citrate restrained the oxidation (Fig. 6a). The Mn(II) passivated mineral surfaces after adsorption (Tani et al. 2004; Parikh et al. 2008; Fischel et al. 2015). The highest concentrations of dissolved Mn in citrate-amended batches might lead to the highest adsorption of dissolved Mn on the surface and inhibited As(III) oxidation, while relatively low concentrations of dissolved Mn in EDTA-amended batches connected to less Mn adsorption and the increase in As(III) oxidation. The highest content of Mn(II) (%) in used birnessite in citrate-birnessite-As(III) batches (Table 3) proves this assumption. It implies that the reaction between citrate/Mn(II)-citrate complex and birnessite occupied more active sites than those produced by the mineral dissolution, which inhibited As(III) oxidation. Moreover, Mn(III) (%) was relatively constant after 1440-min reaction in As(III) control batches (Table 3). Based on the highest content of Mn(III) (%) obtained on used birnessite in citrate-birnessite-As(III) batches (Table 3), this study indicates that citrate and As(III) oxidation might promote the accumulation of MnOOH. In citrate-birnessite-As(V) batches, only citrate and birnessite could undergo redox reactions; the constant Mn(III) (%) of the used birnessite (Table 3) implies that citrate alone had no significant influence on contents of Mn(III) (%) and was unable to accumulate the MnOOH.

For EDTA-amended batches, the highest oxidation rate was obtained (Fig. 6a), where dissolved Mn concentration was higher than that of the control batches (Fig. 6b). The higher concentrations of dissolved Mn indicate that more active sites were created via dissolution. At the beginning of this stage with no detectable dissolved Mn in the control batches, total dissolved Mn was higher, and dissolved Mn(III) in EDTA-birnessite-As(III) batches was slightly higher than those of EDTA-birnessite batches (Fig. 10c, d). This observation indicates that As(III) oxidation increased content of total dissolved Mn and dissolved Mn(III) in EDTA-birnessite-As(III) batches. Since Mn(II) produced by the As(III) oxidation was adsorbed on the birnessite initially (Fischel et al. 2015), the slightly higher dissolved Mn(III) might be caused by the complexation of EDTA which released the adsorbed Mn from the active sites into solution and then accelerated the As(III) oxidation rate.

Table 4 Relative contents of solid Mn species in synthetic birnessite (unreacted), and solid Mn species and dissolved Mn species in As(V) batches (As(V)), citrate-As(V) batches (cit(V)), EDTA-As(V) batches (EDTA(V)), As(III) batches (As(III)), citrate-As(III) batches (cit(III)), and EDTA-As(III) batches (EDTA(III))

Sample	$Mn_{solid\ surface}$ [(b)] (%)[(d)]			$Mn_{solution}$ [(c)] (%)[(d)]	
	Mn(II)	Mn(III)	Mn(IV)	Mn(II)	Mn(III)
Unreacted	3.24	40.49	56.27	-	-
As(V)	1.15	42.30	56.55	-	-
cit(V)	3.51	37.69	58.8	33.94	66.06
EDTA(V)	1.26	40.61	58.13	9.83	90.17
As(III)	3.84	37.28	58.88	100	0
cit(III)	4.51	45.23	50.26	34.77	65.23
EDTA(III)	2.99	41.16	55.85	3.96	96.04

[(b)] $Mn_{solid\ surface}$ refers to the solid Mn species

[(c)] $Mn_{solution}$ refers to the dissolved Mn species

[(d)] The percentage represents the relative contents of solid Mn species in the birnessite obtained from Mn(2p3/2) multi-peak fitting

[(e)] The percentage represents the relative concentration of dissolved Mn(II) and Mn(III) to total dissolved Mn (dissolved Mn(II) + dissolved Mn(III))

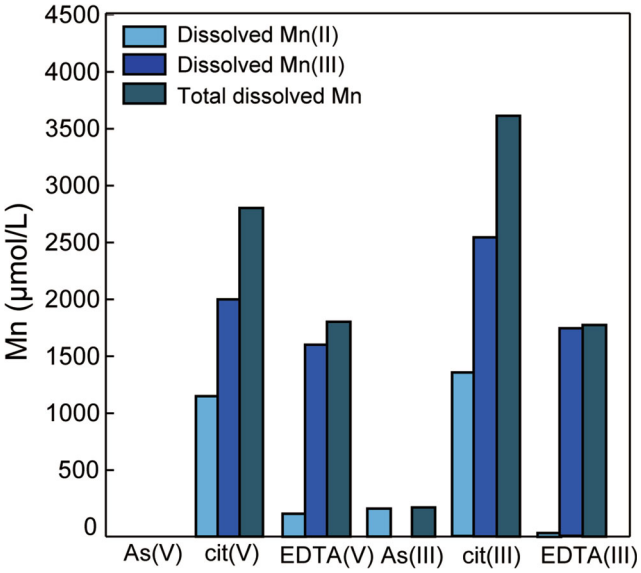

Fig. 11 Total dissolved Mn, dissolved Mn(II), and dissolved Mn(III) concentrations in solutions of As(V) batches (As(V)), citrate-As(V) batches (cit(V)), EDTA-As(V) batches (EDTA(V)), and As(III) batches (As(III), citrate-As(III) batches (cit(III)), EDTA-As(III) batches (EDTA(III)))

Effect of birnessite reduction on As(V) adsorption and As(III) oxidation

Both As(III) and LMWOAs were conducive to dissolution of birnessite. Birnessite in As(III) batches generally experienced the stronger dissolution process than in As(V) batches. The highest amount of birnessite dissolution was found in citrate-amended As(III) batches, followed by EDTA-amended As(III) batches and control batches (Figs. 5b, 6b, and 11; Table 4). The citrate-amended As(III) batches had the highest concentrations of dissolved Mn, while the percentage of Mn(III) in dissolved Mn was the highest in EDTA-amended As(III) batches (Table 4). Speciation of Mn in the used birnessite also supports those observations. The highest Mn(II) (%) of birnessite was found in the citrate-birnessite-As(III) batches, followed by the controls, and the citrate-birnessite-As(V) batches. The used birnessite in the citrate-As(III) batches had the lowest Mn(IV) (%) and the highest Mn(III) (%). Citrate promoted reductive dissolution of birnessite and the accumulation of solid-associated Mn(II) and Mn(III). In relative to controls, EDTA promoted the dissolution of birnessite, but inhibited the aggregation of Mn(II) on the mineral surfaces. Although LMWOAs led to Mn(IV) oxide dissolution, no transformations of the mineral phase occurred (Figs. 7 and 8, and Table 3).

LMWOA-promoted dissolution of birnessite led to the high amount of As(V) adsorption. Higher percentage of dissolved Mn(III) and lower relative contents of Mn(II) on the mineral surface corresponded to more efficient As(V) adsorption (Fig. 5, Tables 3, 4). Dissolution-induced active sites were responsible for higher As adsorption (Parikh et al. 2008; Lafferty et al. 2010a, 2010b) in LMWOA-amended batches. Although more Mn(IV) oxides were dissolved in citrate-As(V) batches, As(V) adsorption was lower than in EDTA-As(V) batches, which may result from the passivation effect of surface Mn(II) (Fig. 5). The highest amount of As(V) adsorption in EDTA-amended batches was likely the result of the limited competitive adsorption of Mn(III)-EDTA complex with As(V) (Prieto et al. 2013).

Although the accumulation of solid-associated Mn(II)/Mn(III) on the mineral surface inhibited As(III) oxidation, higher percentage of dissolved Mn(III) decreased competitive adsorption between As and Mn complex (Fig. 6, Table 2). Higher contents of Mn(II) (%) of the birnessite imply that there was a mineral surface complexation between birnessite and Mn(II)-citrate complex (Wang and Stone 2006b; Jefferson et al. 2015). High contents of Mn(III) (%) might be related to the inadequate As(III) oxidation by MnOOH (Eq. (3)) in the presence of citrate. In EDTA-amended batches, Mn(III) as the predominant dissolved Mn species and the lowest content of Mn(II) (%) in solids suggest that EDTA could activate the birnessite through complexing with adsorbed Mn(II) (Prieto et al. 2013), and thereby promote the As(III) oxidation.

Environmental implications

High concentrations are normally observed in geothermal groundwater (Pope and Brown 2014; Guo et al. 2017). Due to the long-term and large-scale utilization, there is an

increasing risk of allogenic As(III) contamination of As-free aquifers by high As groundwater intrusion (Gillispie et al. 2019). During the intrusion of high As groundwater, the presence of Mn(IV) oxides within aquifer sediments acts as a buffer for As(III) contamination via oxidizing As(III) at a relatively rapid rate. Usually, Fe(III) oxides coexisting with Mn(IV) oxides in aquifers immobilize dissolved As(V) and reduce the possible risks of As contamination to As-free groundwater (Pedersen et al. 2006; Ying et al. 2012). The findings of this study demonstrate that As(III) introduced to aquifers with the presence of Mn(IV) oxides should be oxidized to As(V) effectively, although the reactive surface sites of Mn(IV) oxides are dependent on adsorbed Mn(II) or As(V) (Fischel et al. 2015).

As demonstrated in this study, As(V) was adsorbed relatively effectively on Mn oxides in the presence of LMWOAs since additional surface sites were available on the birnessite after being altered by LMWOAs (such as citrate and EDTA). The extent of alteration was different for different LMWOAs (Banks et al. 2006; Malek et al. 2009). Citrate derives from the plant root exudates (Huangfu et al. 2015), while EDTA is mainly from the anthropogenic input as being used for soil remediation (Kim et al. 2018). Though As behavior is influenced by the quantity and reactivity of LMWOAs in aquifers, it is still difficult to predict geogenic As intrusion to As-free groundwater since these components and phases are naturally variable.

Moreover, interaction between LMWOAs and Mn oxides leads to elevated levels of dissolved Mn concentrations. High concentrations of LMWOAs in water environments resulted in dissolution of Mn oxides (Debela et al. 2010; Wu et al. 2011) with changing the redox properties of Mn oxides-containing soils (Guo and Cutright 2015). Our study shows that LMWOAs increased concentrations of dissolved Mn with low valences, and changed the relative contents of solid-associated low-valent Mn. In the presence of LMWOAs, Mn oxides are firstly reduced, and then Fe oxides are reduced in aquifers, which cause the fact that high dissolved Mn concentrations were coupled with low As concentrations in groundwater (Buschmann et al. 2007). Therefore, high concentrations of dissolved Mn need to be considered in low As groundwater. Elevated Mn concentrations have a negative impact on human health (Wasserman et al. 2006; Buschmann et al. 2007; Marins et al. 2019), which possibly depends on concentration of dissolved Mn(II) (He et al. 2020).

Conclusion

The presence of citrate and EDTA substantially affected As(V) adsorption and As(III) oxidation by birnessite. Both citrate and EDTA promoted As(V) adsorption due to the creation of new active sites by LMWOA-induced reductive dissolution. In comparison with citrate, EDTA was more conducive to As(V) adsorption by forming Mn(III)-EDTA complex in solutions, which suppressed the competitive adsorption of As with dissolved Mn complex. Citrate and EDTA played different roles in As(III) oxidation. In general, citrate inhibited As(III) oxidation and As(V) adsorption, while EDTA promoted As(III) oxidation. The inhibition of As(III) oxidation and adsorption of As(V) in citrate-amended experiments was attributed to competitive adsorption of citrate/Mn(II)-citrate. Promotion of As(III) oxidation by EDTA mainly resulted from increasing the active sites via birnessite dissolution and decreasing the competitive adsorption of dissolved Mn species by forming Mn(III)-EDTA complex. Considering the importance of LMWOAs, further studies need to investigate how their different functional groups affect As behavior in Mn(IV) oxide system.

Funding information The study was financially supported by the National Natural Science Foundation of China (grant nos. 41825017, 41672225, and 41702272), Project 111 (No. B20010), and the Fundamental Research Funds for the Central Universities (grant nos. 2652017165 and 2652017051).

References

Ahmed KAM, Huang KX (2014) Rapid synthesis of novel flowerlike $K_{0.46}Mn_2O_4(H_2O)_{1.4}$ hierarchical architectures and their catalytic degradation of formaldehyde in aqueous solution. Solid State Sci 30:11–16. https://doi.org/10.1016/j.solidstatesciences.2014.02.003

Allard S, Gutierrez L, Fontaine C, Croue JP, Gallard H (2017) Organic matter interactions with natural manganese oxide and synthetic birnessite. Sci Total Environ 583:487–495. https://doi.org/10.1016/j.scitotenv.2017.01.120

Amirbahman A, Kent DB, Curtis GP, Davis JA (2006) Kinetics of sorption and abiotic oxidation of arsenic(III) by aquifer materials. Geochim Cosmochim Acta 70(3):533–547. https://doi.org/10.1016/j.gca.2005.10.036

Banerjee D, Nesbitt HW (2001) XPS study of dissolution of birnessite by humate with constraints on reaction mechanism. Geochim Cosmochim Acta 65(11):1703–1714. https://doi.org/10.1016/S0016-7037(01)00562-2

Banks MK, Schwab AP, Henderson C (2006) Leaching and reduction of chromium in soil as affected by soil organic content and plants. Chemosphere 62(2):255–264. https://doi.org/10.1016/j.chemosphere.2005.05.020

Boumaiza H, Renard A, Robinson MR, Kervern G, Vidal L, Ruby C, Bergaoui L, Coustel R (2019) A multi-technique approach for studying Na triclinic and hexagonal birnessites. J Solid State Chem 272:234–243. https://doi.org/10.1016/j.jssc.2019.02.017

Buschmann J, Berg M, Stengel C, Sampson ML (2007) Arsenic and manganese contamination of drinking water resources in Cambodia: coincidence of risk areas with low relief topography. Environ Sci Technol 41(7):2146–2152. https://doi.org/10.1021/es062056k

Cheng R, Kang M, Zhuang S-T, Shi L, Zheng X, Wang J (2019) Adsorption of Sr(II) from water by mercerized bacterial cellulose

membrane modified with EDTA. J Hazard Mater 364:645–653. https://doi.org/10.1016/j.jhazmat.2018.10.083
Chiu VQ, Hering JG (2000) Arsenic adsorption and oxidation at manganite surfaces. 1. Method for simultaneous determination of adsorbed and dissolved arsenic species. Environ Sci Technol 34(10):2029–2034. https://doi.org/10.1021/es990788p
Debela F, Arocena JM, Thring RW, Whitcombe T (2010) Organic acid-induced release of lead from pyromorphite and its relevance to reclamation of Pb-contaminated soils. Chemosphere 80(4):450–456. https://doi.org/10.1016/j.chemosphere.2010.04.025
Duckworth OW, Sposito G (2005) Siderophore-manganese(III) interactions II. Manganite dissolution promoted by desferrioxamine B. Environ Sci Technol 39(16):6045–6051. https://doi.org/10.1021/es050276c
Duckworth OW, Sposito G (2007) Siderophore-promoted dissolution of synthetic and biogenic layer-type Mn oxides. Chem Geol 242(3–4):497–508. https://doi.org/10.1016/j.chemgeo.2007.05.007
Fischel JS, Fischel MH, Sparks DL (2015) Advances in understanding reactivity of manganese oxides with arsenic and chromium in environmental systems. ACS Symp Ser 1197:1–27. https://doi.org/10.1021/bk-2015-1197.ch001
Flynn ED, Catalano JG (2019) Reductive transformations of layered manganese oxides by small organic acids and the fate of trace metals. Geochim Cosmochim Acta 250:149–172. https://doi.org/10.1016/j.gca.2019.02.006
Gao T-Y, Shen Y-G, Jia Z-H, Qiu G-H, Liu F, Zhang Y-S, Feng X-H, Cai C-F (2015) Interaction mechanisms and kinetics of ferrous ion and hexagonal birnessite in aqueous systems. Geochem Trans 16:16. https://doi.org/10.1186/s12932-015-0031-3
Gheju M, Balcu I, Mosoarca G (2016) Removal of Cr(VI) from aqueous solutions by adsorption on MnO2. J Hazard Mater 310:270–277. https://doi.org/10.1016/j.jhazmat.2016.02.042
Gillispie EC, Matteson AR, Duckworth OW, Neumann RB, Phen N, Polizzotto ML (2019) Chemical variability of sediment and groundwater in a Pleistocene aquifer of Cambodia: implications for arsenic pollution potential. Geochim Cosmochim Acta 245:441–458. https://doi.org/10.1016/j.gca.2018.11.008
Ginder-Vogel M, Landrot G, Jason SF, Donald LS (2009) Quantification of rapid environmental redox processes with quick-scanning x-ray absorption spectroscopy (Q-XAS). Proc Natl Acad Sci U S A 106(38):16124–16128. https://doi.org/10.1073/pnas.0908186106
Guan Y, Sun X-M, Jiang X-D, Sa R, Zhou L, Huang Y, Liu Y-T, Li X-J, Lu R-F, Wang C (2017) The effect of Fe-Mn minerals and seawater interface and enrichment mechanism of ore-forming elements of polymetallic crusts and nodules from the South China Sea. Acta Oceanol Sin 36(6):34–46. https://doi.org/10.1007/s13131-017-1004-4
Guo L, Cutright TJ (2015) Remediation of AMD contaminated soil by two types of reeds. Int J Phytorem 17(4):391–403. https://doi.org/10.1080/15226514.2014.910170
Guo H-M, Wen D-G, Liu Z-Y, Jia Y-F, Guo Q (2014a) A review of high arsenic groundwater in mainland and Taiwan, China: distribution, characteristics and geochemical processes. Appl Geochem 2014(41):196–217. https://doi.org/10.1016/j.apgeochem.2013.12.016
Guo H-M, Zhang D, Wen D-G, Wu Y, Ni P, Jiang Y-X, Guo Q, Li F-L, Zheng H, Zhou Y-Z (2014b) Arsenic mobilization in aquifers of the southwest Songnen basin, P.R. China: evidences from chemical and isotopic characteristics. Sci Total Environ 490:590–602. https://doi.org/10.1016/j.scitotenv.2014.05.050
Guo Q, Planer-Friedrich B, Liu M, Li J, Zhou C, Wang Y (2017) Arsenic and thioarsenic species in the hot springs of the Rehai magmatic geothermal system, Tengchong volcanic region, China. Chem Geol 453:12–20. https://doi.org/10.1016/j.chemgeo.2017.02.010
He J-Q, Zhi H, Hu Q, Meng H, Wang J-H, Feng L (2020) The SPE-assisted europium (III) based complex fluorometric assay for the highly selective and sensitive detection of manganese (II) in water. Talanta 210:120633. https://doi.org/10.1016/j.talanta.2019.120633
Hongve D, Van Hees PAW, Lundström US (2000) Dissolved components in precipitation water percolated through forest litter. Eur J Soil Sci 51(4):667–677. https://doi.org/10.1111/j.1365-2389.2000.00339.x
Hou J-T, Li Y-Z, Mao M-Y, Ren L, Zhao X-J (2014) Tremendous effect of the morphology of birnessite-type manganese oxide nanostructures on catalytic activity. ACS Appl Mater Interfaces 6(17):14981–14987. https://doi.org/10.1021/am5027743
Hou J-T, Luo J-L, Hu Z-Q, Li Y-Z, Mao M-Y, Song S-X, Liao Q-L, Li Q-Z (2016) Tremendous effect of oxygen vacancy defects on the oxidation of arsenite to arsenate on cryptomelane-type manganese oxide. Chem Eng J 306:597–606. https://doi.org/10.1016/j.cej.2016.07.072
Hou J-T, Xiang Y-J, Zheng D, Li Y-Z, Xue S-G, Wu C, Hartley W, Tan W-F (2017) Morphology-dependent enhancement of arsenite oxidation to arsenate on birnessite-type manganese oxide. Chem Eng J 327:235–243. https://doi.org/10.1016/j.cej.2017.06.102
Huangfu X-L, Jiang J, Ma J, Wang Y-A, Liu Y-Z, Lu X-X, Zhang X, Cheng HJ (2015) Reduction-induced aggregation and/or dissolution of MnO2 colloids by organics. Colloids Surf A Physicochem Eng Asp 482:485–490. https://doi.org/10.1016/j.colsurfa.2015.07.006
Jackson BP, Miller WP (2000) Effectiveness of phosphate and hydroxide for desorption of arsenic and selenium species from iron oxides. Soil Sci Soc Am 64(5):1616–1622. https://doi.org/10.2136/sssaj2000.6451616x
Jefferson WA, Hu C-Z, Liu H-J, Qu J-H (2015) Reaction of aqueous Cu-Citrate with MnO2 birnessite: characterization of Mn dissolution, oxidation products and surface interactions. Chemosphere 119:1–7. https://doi.org/10.1016/j.chemosphere.2014.04.039
Johnson KL, McCann CM, Wilkinson JL, Jones M, Tebo BM, West M, Elgy C, Clarke CE, Gowdy C, Hudson-Edwards KA (2018) Dissolved Mn(III) in water treatment works: prevalence and significance. Water Res 140:181–190. https://doi.org/10.1016/j.watres.2018.04.038
Kachhawaha MS, Bhattacharya AK (1962) Electrometric study of the system Mn (II) -Citrate. Z Anorg Allg Chem 315(1–2):104–109. https://doi.org/10.1002/zaac.19623150114
Kim EJ, Jeon EK, Baek K (2018) Role of reducing agent in extraction of arsenic and heavy metals from soils by use of EDTA. Chemosphere 152:274–283. https://doi.org/10.1016/j.chemosphere.2016.03.005
Kwon KD, Refson K, Sposito G (2009) On the role of Mn(IV) vacancies in the photoreductive dissolution of hexagonal birnessite. Geochim Cosmochim Acta 73(14):4142–4150. https://doi.org/10.1016/j.gca.2009.04.031
Lafferty BJ, Loeppert RH (2005) Methyl arsenic adsorption and desorption behavior on iron oxides. Environ Sci Technol 39(7):2120–2127. https://doi.org/10.1021/es048701+
Lafferty BJ, Ginder-Vogel M, Sparks D (2010a) Arsenite oxidation by a poorly crystalline manganese-oxide 1. Stirred-flow experiments. Environ Sci Technol 44(22):8460–8466. https://doi.org/10.1021/es102013p
Lafferty BJ, Ginder-Vogel M, Zhu M-Q, Livi KJT, Sparks DL (2010b) Arsenite oxidation by a poorly crystalline manganese-oxide. 2. Results from X-ray absorption spectroscopy and X-ray diffraction. Environ Sci Technol 44(22):8467–8472. https://doi.org/10.1021/es102016c
Lafferty BJ, Ginder-Vogel M, Sparks DL (2011) Arsenite oxidation by a poorly-crystalline manganese oxide. 3. Arsenic and manganese desorption. Environmental ence & Technology 45(21):9218–23. https://doi.org/10.1021/es201281u
Li X-J, Liu C-S, Li F-B, Li Y-T, Zhang L-J, Liu C-P, Zhou Y-Z (2010) The oxidative transformation of sodium arsenite at the interface of alpha-MnO2 and water. J Hazard Mater 173(1–3):675–681. https://doi.org/10.1016/j.jhazmat.2009.08.139

Li Y, Liu F-F, Xu X-M, Liu Y-W, Li Y-Z, Ding H-R, Chen N, Yin H, Lin H, Wang C-Q, Lu A-H (2019) Influence of heavy metal sorption pathway on the structure of biogenic birnessite: insight from the band structure and photostability. Geochim Cosmochim Acta 256: 116–134. https://doi.org/10.1016/j.gca.2018.12.008

Liang M-Y, Guo H-M, Xiu W (2019) Mechanisms of arsenite oxidation and arsenate adsorption by a poorly crystalline manganese oxide in the presence of low molecular weight organic acids. E3S Web of Conferences 98, 04009

Ling FT, Post JE, Heaney PJ, Kubicki JD, Santelli CM (2017) Fourier-transform infrared spectroscopy (FTIR) analysis of triclinic and hexagonal birnessites. Spectrochim Acta A 178:32–46. https://doi.org/10.1016/j.saa.2017.01.032

Liu R-P, Liu H-J, Qiang Z-M, Qu J-H, Li G-B, Wang D-S (2009) Effects of calcium ions on surface characteristics and adsorptive properties of hydrous manganese dioxide. J Colloid Interface Sci 331(2):275–280. https://doi.org/10.1016/j.jcis.2008.11.051

Liu L-H, Tan W-F, Suib SL, Qiu G-H, Zheng L-R, Su S-M (2019) Enhanced adsorption removal of arsenic from mining wastewater using birnessite under electrochemical redox reactions. Chem Eng J:375. https://doi.org/10.1016/j.cej.2019.122051

Luther GW, Madison AS, Mucci A, Sundby B, Oldham VE (2015) A kinetic approach to assess the strengths of ligands bound to soluble Mn(III). Mar Chem 173:93–99. https://doi.org/10.1016/j.marchem.2014.09.006

Madison AS, Tebo BM, Luther GW (2011) Simultaneous determination of soluble manganese(III), manganese(II) and total manganese in natural (pore)waters. Talanta 84(2):374–381. https://doi.org/10.1016/j.talanta.2011.01.025

Madurga S, Nedyallcova M, Mas F, Garces JL (2017) Ionization and conformational equilibria of citric acid: delocalized proton binding in solution. J Phys Chem A 121(31):5894–5906. https://doi.org/10.1021/acs.jpca.7b05089

Malek A, Hachemi M, Didier V (2009) New approach of depollution of solid chromium leather waste by the use of organic chelates: economical and environmental impacts. J Hazard Mater 170(1):156–162. https://doi.org/10.1016/j.jhazmat.2009.04.118

Manceau A, Lanson B, Drits VA (2002) Structure of heavy metal sorbed birnessite. Part III: results from powder and polarized extended X-ray absorption fine structure spectroscopy. Geochim Cosmochim Acta 66(15):2639–2663. https://doi.org/10.1016/S0016-7037(02)00869-4

Marins K, Lazzarotto LMV, Boschetti G, Bertoncello KT, Zanatta L (2019) Iron and manganese present in underground water promote biochemical, genotoxic, and behavioral alterations in zebrafish (danio rerio). Environ Sci Pollut Res 26(1):23555–23570. https://doi.org/10.1007/s11356-019-05621-0

Mock RP, Schaefer MV, Pacheco JL, Lake L, Lee I, Ying SC (2019) Influence of Fe(II) on arsenic(III) oxidation by birnessite in diffusion-limited systems. ACS Earth Space Chem 3(4):550–561. https://doi.org/10.1021/acsearthspacechem.8b00184

Nesbitt HW, Canning GW, Bancroft GM (1998) XPS study of reductive dissolution of 7 angstrom-birnessite by H3AsO3, with constraints on reaction mechanism. Geochim Cosmochim Acta 62(12):2097–2110. https://doi.org/10.1016/S0016-7037(98)00146-X

Oldham VE, Owings SM, Jones MR, Tebo BM, Luther GW (2015) Evidence for the presence of strong Mn(III)-binding ligands in the water column of the Chesapeake Bay. Mar Chem 171:58–66. https://doi.org/10.1016/j.marchem.2015.02.008

Oldham VE, Miller MT, Jensen LT, Luther GW (2017a) Revisiting Mn and Fe removal in humic rich estuaries. Geochim Cosmochim Acta 209:267–283. https://doi.org/10.1016/j.gca.2017.04.001

Oldham VE, Mucci A, Tebo BM, Luther GW (2017b) Soluble Mn(III)-L complexes are abundant in oxygenated waters and stabilized by humic ligands. Geochim Cosmochim Acta 199:238–246. https://doi.org/10.1016/j.gca.2016.11.043

Oscarson DW, Huang PM, Liaw WK, Hammer UT (1983) Kinetics ofoxidation of arsenite by various manganese dioxides. Soil Sci Soc Am J 47(4):644–648. https://doi.org/10.2136/sssaj1983.03615995004700040007x

Owings SM, Luther GW, Taillefert M (2019) Development of a rate law for arsenite oxidation by manganese oxides. Geochim Cosmochim Acta 250:251–267. https://doi.org/10.1016/j.gca.2019.02.003

Pankratova AB, Nevskaya EY, Kutepov AM, Gorichev IG, Izotov AD, Zaitsev BE (2001) Dissolution kinetics of manganese(III, IV) oxides in sulfuric acid in the presence of ethylenediaminetetraacetic acid. Theor Found Chem Eng 35(2):168–174. https://doi.org/10.1023/A:1010385724457

Parikh SJ, Lafferty BJ, Sparks DL (2008) An ATR-FTIR spectroscopic approach for measuring rapid kinetics at the mineral/water interface. Colloid Interface Sci 320(1):177–185. https://doi.org/10.1016/j.jcis.2007.12.017

Parikh SJ, Lafeerty BJ, Meade TG, Sparks DL (2010) Evaluating environmental influences on AsIII oxidation kinetics by a poorly crystalline Mn-oxide. Environ Sci Technol 44(10):3772–3778. https://doi.org/10.1021/es903408g

Pedersen HD, Postma D, Jakobsen R (2006) Release of arsenic associated with the reduction and transformation of iron oxides. Geochim Cosmochim Acta 70(16):4116–4129. https://doi.org/10.1016/j.gca.2006.06.1370

Petrick JS, Ayala-Fierro F, Cullen WR, Carter DE, Aposhian HV (2000) Monomethylarsonous acid (MMA(III)) is more toxic than arsenite in Chang human hepatocytes. Toxicol Appl Pharm 163(2):203–207. https://doi.org/10.1006/taap.1999.8872

Pope J, Brown K (2014) Geochemistry of discharge at Waiotapu geothermal area, New Zealand-trace elements and temporal changes. Geothermics 51:253–269

Prieto C, Lozano JC, Rodriguez PB, Tome FV (2013) Enhancing radium solubilization in soils by citrate, EDTA, and EDDS chelating amendments. J Hazard Mater 250:439–446. https://doi.org/10.1016/j.jhazmat.2013.02.021

Scott MJ, Morgan JJ (1995) Reactions at oxide surfaces. 1. Oxidation of As(III) by synthetic birnessite. Environ Sci Technol 29(8):1898–1905. https://doi.org/10.1021/es00008a006

Si W-Z, Wang Y, Peng Y, Li X, Li K-Z, Li J-H (2015) A high-efficiency γ-MnO2-like catalyst in toluene combustion. Chem Commun 51(81):14977–14980. https://doi.org/10.1039/C5CC04528B

Stone AT, Ulrich HJ (1989) Kinetics and reaction stoichiometry in the reductive dissolution of manganese(IV) dioxide and Co(III) oxide by hydroquinone. Colloid Interface Sci 132(2):509–522. https://doi.org/10.1016/0021-9797(89)90265-8

Strathmann TJ (2011) Redox reactivity of organically complexed iron(II) species with aquatic contaminants. ACS Sym Ser 1071:283–313. https://doi.org/10.1021/bk-2011-1071.ch014

Sun Q, Cui P-X, Liu C, Peng S-M, Alves M-E, Zhou D-M, Shi Z-Q, Wang Y-J (2019) Antimony oxidation and sorption behavior on birnessites with different properties (delta-MnO2 and triclinic birnessite). Environ Pollut 246:990–998. https://doi.org/10.1016/j.envpol.2018.12.027

Swetha JV, Parse H, Kakade B (2018) Morphology dependent facile synthesis of manganese oxide nanostructures for oxygen reduction reaction. Solid State Ionics 328:1–7. https://doi.org/10.1016/j.ssi.2018.11.002

Tani Y, Miyata N, Ohashi M, Ohnuki T, Seyama H, Iwahori K, Soma M (2004) Interaction of inorganic arsenic with biogenic manganese oxide produced by a Mn-oxidizing fungus, strain KR21-2. Environ Sci Technol 38(24):6618–6624. https://doi.org/10.1021/es049226i

Tournassat C, Charlet L, Bosbach D, Manceau A (2002) Arsenic(III) oxidation by birnessite and precipitation of manganese(II) arsenate. Environ Sci Technol 36(3):493–500. https://doi.org/10.1021/es0109500

Villalobos M, Escobar-Quiroz IN, Salazar-Camacho C (2014) The influence of particle size and structure on the sorption and oxidation behavior of birnessite: I. adsorption of As(V) and oxidation of As(III). Geochim Cosmochim Acta 125:564–581. https://doi.org/10.1016/j.gca.2013.10.029

Wang Y, Stone AT (2006a) Reaction of MnIII,IV(hydr)oxides with oxalic acid, glyoxylic acid, phosphonoformic acid, and structurally-related organic compounds. Geochim Cosmochim Acta 70: 4477–4490. https://doi.org/10.1016/j.gca.2006.06.1548

Wang Y, Stone AT (2006b) The citric acid–MnIII,IVO_2(birnessite) reaction. Electron transfer, complex formation, and autocatalytic feedback. Geochim Cosmochim Acta 70:4463–4476. https://doi.org/10.1016/j.gca.2006.06.1551

Wang Y, Feng X-H, Villalobos M, Tan W-F, Liu F (2012) Sorption behavior of heavy metals on birnessite: relationship with its Mn average oxidation state and implications for types of sorption sites. Chem Geol 292:25–34. https://doi.org/10.1016/j.chemgeo.2011.11.001

Wang N, Liang C, Du L, Cui H (2013) Arsenite sorption and oxidation by synthetic birnessite. J Water Supply Res Technol Aquat 62(4):245–253. https://doi.org/10.2166/aqua.2013.099

Wang H-W, Zhang D-Y, Mou S, Song W, Al-Misned FA, Mortuza MG, Pan X-L (2015) Simultaneous removal of tetracycline hydrochloride and As(III) using poorly-crystalline manganese dioxide. Chemosphere 136:102–110. https://doi.org/10.1016/j.chemosphere.2015.04.070

Wang Q, Liao X-Y, Xu W-Q, Ren Y, Livi KJT, Zhu M-Q (2016) Synthesis of birnessite in the presence of phosphate, silicate, or sulfate. Inorg Chem 55(20):10248–10258. https://doi.org/10.1021/acs.inorgchem.6b01465

Wang H-W, Wang Y-N, Sun Y-J, Tsang Y-F, Zhang D-Y, Pan X-L (2017) A microscopic and spectroscopic study of rapid antimonite sequestration by a poorly crystalline phyllomanganate: differences from passivated arsenite oxidation. RSC Adv 7(61):38377–38386. https://doi.org/10.1039/c7ra05939f

Wang H-W, Wang Y-N, Sun Y-J, Pan X-L, Zhang D-Y, Tsang Y-F (2018a) Differences in Sb(V) and As(V) adsorption onto a poorly crystalline phyllomanganate (delta-MnO2): adsorption kinetics, isotherms, and mechanisms. Process Saf Environ Protect 113:40–47. https://doi.org/10.1016/j.psep.2017.09.015

Wang Q, Yang P, Zhu M-Q (2018b) Structural transformation of birnessite by fulvic acid under anoxic conditions. Environ Sci Technol 52(4):1844–1853. https://doi.org/10.1021/acs.est.7b04379

Wasserman GA, Liu X-H, Parvez F, Ahsan H, Levy D, Factor-Litvak P, Kline J, van Geen A, Slavkovich V, Lolacono NJ, Cheng Z-Q, Zheng Y, Graziano JH (2006) Water manganese exposure and children's intellectual function in Araihazar, Bangladesh. Environ Health Perspect 114(1):124–129. https://doi.org/10.1289/ehp.8030

Winkel LHE, Casentini B, Bardelli F, Voegelin A, Nikolaidis NP, Charlet L (2013) Speciation of arsenic in Greek travertines: co-precipitation of arsenate with calcite. Geochim Cosmochim Acta 106:99–110. https://doi.org/10.1016/j.gca.2012.11.049

Wu Y-Y, Zhou S-Q, Ye X-Y, Chen D-Y, Zheng K, Qin F-H (2011) Transformation of pollutants in landfill leachate treated by a combined sequence batch reactor, coagulation, Fenton oxidation and biological aerated filter technology. Process Saf Environ Prot 89(2):112–120. https://doi.org/10.1016/j.psep.2010.10.005

Ying SC, Kocar BD, Fendorf S (2012) Oxidation and competitive retention of arsenic between iron-and manganese oxides. Geochim Cosmochim Acta 96:294–303. https://doi.org/10.1016/j.gca.2012.07.013

Zhang T, Sun D-D (2013) Removal of arsenic from water using multi-functional micro−/nano-structured MnO2 spheres and microfiltration. Chem Eng J 225:271–279. https://doi.org/10.1016/j.cej.2013.04.001

Zhang L-M, Liu F, Tan W-F, Feng X-H, Zhu Y-G, He J (2008) Microbial DNA extraction and analyses of soil iron-manganese nodule. Soil Biol Biochem 40(6):1364–1369. https://doi.org/10.1016/j.soilbio.2007.01.004

Zhang S, Chen S-F, Liu F, Li J-S, Liang X-L, Chu S-Q, Xiang Q-J, Huang C-Q, Yin H (2018a) Effects of Mn average oxidation state on the oxidation behaviors of As(III) and Cr(III) by vernadite. Appl Geochem 94:35–45. https://doi.org/10.1016/j.apgeochem.2018.05.002

Zhang C, Wang S, Cao Z-F, Zhong H (2018b) A novel process for the separation and recovery of value-added metals from manganese-silver ores by EDTA/EDTA-2Na and thiosulfate. Hydrometallurgy 178:256–263. https://doi.org/10.1016/j.hydromet.2018.05.007

Zhao H-Y, Zhu M-Q, Li W, Elzinga EJ, Villalobos M, Liu F, Zhang J, Feng X-H, Sparks DL (2016) Redox reactions between Mn(II) and hexagonal birnessite change its layer symmetry. Environ Sci Technol 50(4):1750–1758. https://doi.org/10.1021/acs.est.5b04436

Zheng H, Zhang Q, Liu G-C, Luo X-X, Li F-M, Zhang Y-P, Wang Z-Y (2019) Characteristics and mechanisms of chlorpyrifos and chlorpyrifos-methyl adsorption onto biochars: influence of deashing and low molecular weight organic acid (LMWOA) aging and co-existence. Sci Total Environ 657:953–962. https://doi.org/10.1016/j.scitotenv.2018.12.018

Zhu M-Q, Gindervogel M, Parikh SJ, Feng X-H, Sparks DL (2010) Cation effects on the layer structure of biogenic Mn-oxides. Environ Sci Technol 44:4465–4471. https://doi.org/10.1021/es1009955